Hybrid NS-DSMC simulation of a full scale solid rocket motor reactive exhaust at high altitude

Antoine Clout, Adrien Langenais, Dauvois Yann, Mieussens Luc, Julien Labaune

DOI:

Hybrid NS-DSMC simulation of a full scale solid rocket motor reactive exhaust at high altitude

Antoine Clout[⋆†], *Adrien Langenais*[⋆], *Yann Dauvois*[⋆⋆], *Luc Mieussens*[⋆⋆⋆], *Julien Labaune*[⋆]
[⋆]*DMPE, ONERA, Université Paris Saclay, F-91123 Palaiseau - France*
[⋆⋆]*ONERA / DMPE, Université de Toulouse, F-31055 Toulouse - France*
[⋆⋆⋆]*Bordeaux INP, Univ. Bordeaux, CNRS, IMB, UMR 5251, F-33400 Talence, France*
antoine.clout@onera.fr
[†]Corresponding author

Abstract

The present work uses a hybrid methodology to simulate a multispecies flow exhausting from the JAXA's M-V third stage at an altitude of 183km. The methodology couples a Navier-Stokes (NS) solver for the rocket plume with a Direct-Simulation Monte-Carlo (DSMC) solver for the low pressure atmosphere in a one-way approach. A dedicated solver is used to simulate alumina particles and their interaction with the gas. The multiscale and multiphysics nature of the studied case induced numerical difficulties in the DSMC resolution which were tackled for instance by limiting the minimum cell size in the DSMC solver adaptive mesh refinement. A hybrid NS-DSMC full-scale simulation was performed and showed better capture of H_2 expansion towards the front of the vehicle than the NS only approach.

Nomenclature and abbreviations

Symbol	Meaning	Unit
γ	Heat capacity ratio	[−]
κ	Thermal conductivity	$\left[\mathrm{W\,m^{-1}\,K^{-1}}\right]$
λ	Mean free path	[m]
μ	Dynamic viscosity	[Pa s]
ρ	Density	$\left[\mathrm{kg\,m^{-3}}\right]$
σ	Surface tension	$\left[\mathrm{J\,m^{-2}}\right]$
χ	Accommodation parameter	[−]
x	Axial position	[m]
r	Radial position	[m]
n	Normal direction	[−]
τ	Tangential direction	[−]
Ma	Mach number	[−]
We	Weber number	[−]
Kn	Knudsen number	[−]
Pr	Prandlt number	[−]
Ra	Rarefaction criterion	[−]

Symbol	Meaning	Unit
D	Particle diameter	[m]
$\mathrm{f_{num}}$	Ratio of physical molecules to simulation particles	[−]
k_B	Boltzmann constant	$\left[\mathrm{m^2\,kg\,s^{-2}\,K^{-1}}\right]$
p	Pressure	[Pa]
R	Ideal gas constant	$\left[\mathrm{J\,K^{-1}\,mol^{-1}}\right]$
$\mathrm{R_{specific}}$	Specific gas constant	$\left[\mathrm{J\,K^{-1}\,kg^{-1}}\right]$
T	Temperature	[K]
u	Velocity	$\left[\mathrm{m\,s^{-1}}\right]$
Y_k	Mass fraction of species k	[−]

Abbreviation	Meaning
NS	Navier-Stokes
DSMC	Direct-Simulation Monte-Carlo

1. Introduction

Simulating the flowfield in the plume of a rocket motor is critical to ensure smooth running of a mission. For instance, the ionisation in the plume can interact with radio frequency waves and cause communication blackout as studied for instance by Kinefuchi *et al.* [1]. Another important aspect is the heat and particles fluxes on the launcher base that can occur due to the plume flowing upstream in some atmospheric conditions. These fluxes can challenge the structural integrity of the rocket or degrade critical equipment [2].

In the lower layers of the atmosphere, computing the plume and surrounding flowfields can be done by solving the Navier-Stokes (NS) equations with a finite volume method. Reynolds-Averaged Navier-Stokes (RANS) or Large-

Eddy Simulation (LES) approaches [3] can be used. The NS equations can be derived from the Boltzmann transport equation (BTE) describing the kinetic theory of gases on a microscopic level, using the assumptions that the fluid is continuous and that the molecules are in local thermal equilibrium. As the altitude increases, the density of the atmosphere decreases, and the mean free path of the molecules becomes comparable to the characteristic length scales of the flow. The fluid can then no longer be considered continuous, and the NS equations break down. The precise altitude at which the NS equations stop being valid is not a consensus in the literature [4].

In order to simulate the plume flowfield, several methods are used. Some authors still use the NS equations regardless of the error, and use some corrections determined empirically to compute for instance the electron density behind the launcher [1]. This method can give rather accurate results but cannot be generalized easily. A solution to extend the domain of validity of the equations is to derive higher order equations, *i.e.* use higher order terms in the derivation from the BTE. These are for example the Burnett and Super-Burnett equations [5]. These equations do not accurately describe the multi-temperature effects inside shocks [6]. The BTE being extremely costly to solve directly, other models such as the *Bhatnagar, Gross and Krook* (BGK) model [7] have been developed. It consists in a simplification of the collision term in the BTE which results in a huge decrease in computational time. This approach has been assessed in the context of wall pollution of outgassing spacecraft [8], but experimental results are still lacking to make firm conclusions. This model is also used for atmospheric reentry [9], which shares the hypersonic and rarefied aspects with high altitude plume simulation. Another strategy is to solve the BTE using a Direct-Simulation Monte-Carlo (DSMC) stochastic method [10]. Numerical particles are directly simulated in a Lagrangian framework, with propagation and collisions in each mesh cell. It is accurate even at very low densities but its computational cost scales as the mean free path λ^{-4}, so it becomes really expensive when the flow is densifying. For plume simulation at high altitude both high and low densities, in the combustion chamber and outside the spacecraft respectively, are encountered, therefore the applicability of the DSMC method is limited.

Hybrid methods have been developed to solve this issue. They consist in having two separate solvers, one for the continuous region and one for the rarefied region. In one-way coupled methods, a continuous solution using a finite volume NS solver is computed on the whole domain, an interface corresponding to the end of validity of the NS equations is determined and used as an input condition for a rarefied solver, *e.g.* using the DSMC method. This has been applied to micro-thrusters [11], to decimetric-sized thrusters [12] and to sounding rockets [13]. Another approach is to have a two-way coupling between the continuous and rarefied solvers. Both solvers are run iteratively, using the output of one as the input for the next iteration of the other. It has been used for academic and re-entry hypersonic flows [4, 14, 15], then for rocket plume flows, particularly for small thrust engine [16–18], but also for military applications [19]. A review of the authors using this method for electric and chemical plumes has been written by Cai *et al.* [20]. The method is also used in other fields of research, for example in isotope separation simulation [21].

In this paper, a simulation using a one-way coupling method between a finite volume Navier-Stokes solver and a DSMC solver is performed on a full scale orbital rocket at high altitude. The one-way approach is preferred compared to the two-way coupling due to its ease of implementation, which has been done at ONERA by Charton *et al.* [11]. This multi-scale situation induces new challenges compared to previous works [11, 12]. First the rarefaction of the atmosphere induces velocity and temperature jumps at the walls of the rocket which modify the flowfield in its vicinity. The increase in mean free path translates into a thickening of the front bow shock, increasing the required axial length of the domain. Due to the large range of densities, robustness of the solvers are also a concern. Finally the chemical composition of the exhaust implies propagation of several species which increases the computational cost. The case studied is the third stage of JAXA's M-V rocket [22], depicted in Figure 1. The altitude of simulation is 183 km and the vehicle velocity is 6100 m s^{-1}. The chamber pressure of this solid rocket motor is 5.6 MPa and the propellant used is an ammonium perchlorate / hydroxyl-terminated polybutadiene (AP/HTPB) composite solid propellant containing 20 % of aluminum in mass [23].

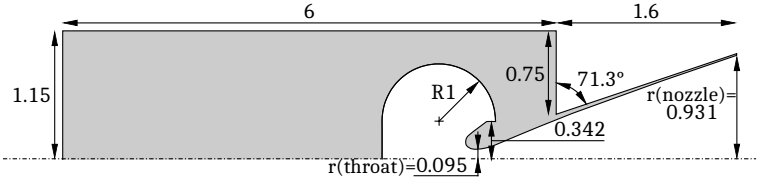

Figure 1: JAXA's M-V 3rd stage geometry [23]. Dimensions are in meters and angles in degrees.

The paper is organized as follows. The numerical simulation methodology is presented in Section 2, with a description of the general coupling principle, a description of both solvers and a discussion on the rarefaction criterion defining the end of validity of the NS equations. Section 3 then presents all the simulation results, first for the NS based simulation, then for a simplified case where several interfaces are evaluated, and finally a general comparison of the

hybrid method compared to the NS only solution. Concluding remarks are given in Section 4.

2. Numerical simulation methodology

2.1 General coupling principle

The Navier-Stokes - Direct-Simulation Monte-Carlo method (NS-DSMC) one-way coupling principle relies on the following steps:

- A flow solution is computed by solving the NS equations on the whole simulation domain. The flow is supposed to be continuous and the solution is used as an input for the following steps. The associated numerical parameters are detailed in Section 2.2.
- A rarefaction criterion Ra is computed using the previous results. The mathematical expression of the criterion used in this paper is discussed in Section 2.3. A Ra isoline is drawn along a specified threshold value. A continuous domain and a rarefied domain are thus identified, *i.e.* wherever $Ra<Ra_{threshold}$ and $Ra>Ra_{threshold}$ respectively.
- The isoline, denoted "interface" in the following, is discretized into segments. Flow temperature, density and velocity are extracted along these segments.
- A rarefied simulation using the DSMC method is performed over the rarefied domain, taking the interface as input. The associated numerical parameters are detailed in Section 2.4.

These steps are illustrated in Figure 2. One hypothesis about the one-way coupling methodology is the absence of feedback from the rarefied domain on the continuous domain. This translates into the need for supersonic normal velocity at any point on the interface, *i.e.* u_n shall be supersonic everywhere along the interface, depicted in blue in Figure 2. This condition is problematic due to two reasons. First, very close to the nozzle, the wall friction implies that the fluid is subsonic, and information could be transferred from the rarefied to the continuous domain in this region. Secondly due to the small angle between the streamlines and the interface close the rocket base, having a supersonic normal velocity can be challenging.

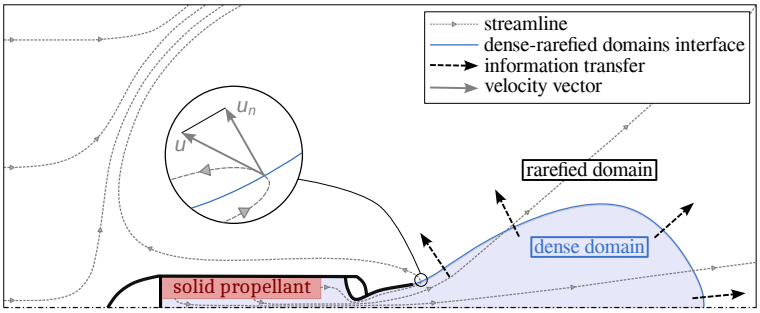

Figure 2: General NS-DSMC one-way coupling methodology principle.

2.2 Continuous flow solver

The multi-physics computational fluid dynamics (CFD) code CEDRE is utilized as continuous flow solver [24]. It employs a finite volume approach on generalized unstructured meshes.

The gas solver addresses the NS balance equations for mass, chemical species mass fractions, momentum, and energy, encompassing convection, molecular diffusion, and chemical reaction. Reynolds-Averaged Navier-Stokes (RANS) simulations are conducted with a k-ω closure model. The turbulence Reynolds stresses are modeled using the Boussinesq approximation. The inviscid fluxes are computed using the Harten-Lax-van Leer contact approximate Riemann solver to handle non-smooth solutions such as shock waves. Second-order accuracy is achieved by employing variable extrapolation through the monotonic upwind scheme for conservation laws (MUSCL), in conjunction with van Leer flux limiters to ensure the numerical scheme's monotonicity. The viscous fluxes are evaluated using a second-order centered scheme. The time integration is performed using a first order implicit scheme. Extensive verification of the CEDRE solver has been conducted using well-established numerical benchmarks [24, 25].

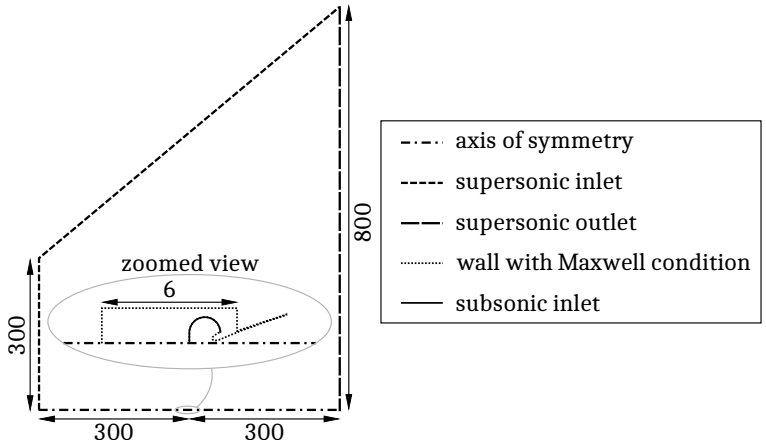

Figure 3: Domain size and boundary conditions used in the continuous simulation. The ellipse corresponds to a zoomed view. Dimensions are in meters.

The 2D axisymmetric simulated domain is depicted in Figure 3. Due to the rarefied atmosphere, the bow shock in front of the stage is expected to be several tens or hundreds of meter thick, which explains the 300 m long upstream domain. The left and top boundary conditions are supersonic inlets at atmospheric conditions. The right boundary condition is a supersonic outlet, *i.e.* it has no action of the flow. The combustion chamber in the rocket is set as a subsonic inlet, with burnt gases and alumina particles injection. The other walls, denoted *wall with Maxwell condition* in Figure 3, use an adiabatic Maxwell-Smoluchowski [26] wall condition. When the flow is dense, this condition tends to a no slip condition and the temperature jump tends to 0. As the flow becomes rarefied, the slip velocity increases. The velocity and temperature differences between the first layer of fluid and the wall [27] are:

$$u_{\text{fluid}} - u_{\text{wall}} = \alpha_1 \frac{2-\chi}{\chi} \lambda \frac{\partial u}{\partial n} + \frac{\alpha_2}{2\text{Pr}} \frac{\mu}{\rho T} \frac{\partial T}{\partial \tau} \tag{1}$$

$$T_{\text{fluid}} - T_{\text{wall}} = \beta_1 \frac{2-\chi}{\chi} \frac{2\gamma}{(\gamma+1)\text{Pr}} \lambda \frac{\partial T}{\partial n} + \beta_2 \frac{M}{R} \frac{\mu}{6\rho} \left(2 \frac{\partial u_n}{\partial n} - \frac{\partial u_\tau}{\partial \tau} \right) \tag{2}$$

where n is the wall normal direction, τ the tangential direction, μ the dynamic viscosity of the flow, ρ its density, γ its heat capacity ratio, λ its local mean free path, Pr its Prandtl number, M is the molar mass of the gas, R the ideal gas constant, χ an accommodation parameter which is set to 1 based on an optimization study [28], and finally according to Struchtrup [27]:

$$\alpha_1 = \frac{\chi}{2-\chi} \frac{2}{\sqrt{\pi}} \sigma_p \qquad \alpha_2 = \frac{4}{3} \sigma_T \qquad \beta_1 = \frac{\chi}{2-\chi} \frac{16}{15\sqrt{\pi}} \zeta_T \tag{3}$$

with $\beta_2 = 1$, $\sigma_p = 0.987$, $\sigma_T = 1.009$, and $\zeta_T = 1.873$. With no information on the wall temperature, the condition is set as adiabatic by imposing $T_{\text{fluid}} - T_{\text{wall}} = 0$. A in-house wall law is also used to model the wall friction. The simulation is performed using a time step of 1×10^{-7} s and only the steady state solution is of interest.

Due to the presence of aluminum in the solid propellant, the plume contains alumina particles which have a first order influence on the gas phase. A dedicated in-house condensed phase solver is used [24], with an Eulerian framework that allows for injection, transport and interaction with the gaseous phase of condensed phase particles, including fusion and solidification due to heat transfer. The spatial interpolation is done using a second order scheme with van Leer flux limiters and a Godunov scheme. The time integration is performed using a first order implicit scheme. The two solvers for gaseous and condensed phases are strongly coupled, and the numerical parameters for each are described in Section 2.2.1 and Section 2.2.2 respectively.

2.2.1 Gas phase numerical parameters

Two different mixtures are injected along the two inlet boundary conditions. The first mixture corresponds to the atmospheric condition imposed in the left boundary of the domain. At 183 km, the composition of the atmosphere is as in Table 1, according to the U.S. Standard atmosphere [29]. This air mixture is injected at a velocity of 6100 m s^{-1} in the x direction, at a static pressure of 1.39×10^{-4} Pa and a temperature of 801 K.

The second mixture is composed of burnt solid propellant gases. The composition of the 14 species mixture is the result of a zero-dimensional thermochemical equilibrium simulation of the combustion of a 68 % AP, 12 % HTPB

Table 1: Mass fraction of the atmospheric gases injected through the supersonic inlet.

N_2	O_2	O
0.593 91	0.048 73	0.357 36

and 20 % aluminum simplified solid propellant, and is detailed in Table 2. The gas mass flow rate is $60\,\mathrm{kg\,s^{-1}}$. The injection temperature is 3530 K. The turbulent intensity is set to 0.2 and the characteristic turbulent length-scale to r(nozzle)/10, with r(nozzle) the nozzle exit radius as depicted in Figure 1.

Table 2: Mass fraction of the burnt gases injected in the combustion chamber.

N_2	O_2	H_2	H_2O	H	O	OH
0.212 551	0.000 156	0.034 173	0.105 557	0.002 52	0.000 571	0.007 038

CO	CO_2	HCl	Cl_2	Cl	Na	NaCl
0.347 327	0.023 512	0.242 977	7.4×10^{-5}	0.023 286	1.8×10^{-5}	0.000 24

The simulation includes the same kinetic scheme as in Charton *et al.* [12], composed of 24 chemical reactions taking into account both gas expansion and ionization. The specific heat of each species is determined with seventh order polynomials generated from data fitting between 0 K and 20 000 K of several data bases including NIST, NASA9 and Capitelli *et al.* [30].

2.2.2 Condensed phase numerical parameters

The physical properties of the injected alumina particles are taken from Binauld *et al.* [31]. The specific heat coefficient of both liquid and solid phase are approximated using a third order polynomial according to the following Equation (4).

$$c_p(T) = c_0 + c_1 \frac{T}{T_0} + c_2 \left(\frac{T}{T_0}\right)^2 + c_3 \left(\frac{T}{T_0}\right)^3 \tag{4}$$

with $T_0 = 1000\,\mathrm{K}$ and the polynomial coefficients are given in Table 3.

Table 3: Heat capacity polynomial coefficients of the Al_2O_3 particules.

	c_0	c_1	c_2	c_3
Solid phase $\left[\mathrm{J\,kg^{-1}\,K^{-1}}\right]$	461.32	1489.5	-894.27	182.9
Liquid phase $\left[\mathrm{J\,kg^{-1}\,K^{-1}}\right]$	1887.64	0	0	0

The density is $2700\,\mathrm{kg\,m^{-3}}$ for both phases. The solidification temperature is 2327 K. The particles are injected at the boundary condition in thermal and dynamic equilibrium with the gaseous phase. The diameter distribution of the alumina particles in the combustion chamber is not known, therefore a log-normal distribution with a de Brouckere mean diameter D_{43} of 7 µm, inferred as in [32] from Hermsen's correlations [33], and a standard deviation of 1 µm is assumed. Figure 4 shows in red the probability density function of the diameters of the alumina particle and in blue the corresponding cumulative density function. A discretization in 7 discrete independent classes is made, as shown in Table 4. Each class of particles represents a range of diameters but is only represented by one specific diameter. The corresponding injected mass flux is also in Table 4. The total particle mass flux is $30.4\,\mathrm{kg\,s^{-1}}$ which corresponds to around a third of the total mass flux.

2.3 Rarefaction criterion

On the basis of the continuous NS flow solution, a limit of validity may be defined. Several parameters are used as a rarefaction criterion in the literature, the two main ones being the gradient length local Knudsen numbers $\mathrm{Kn_{GLL}}$

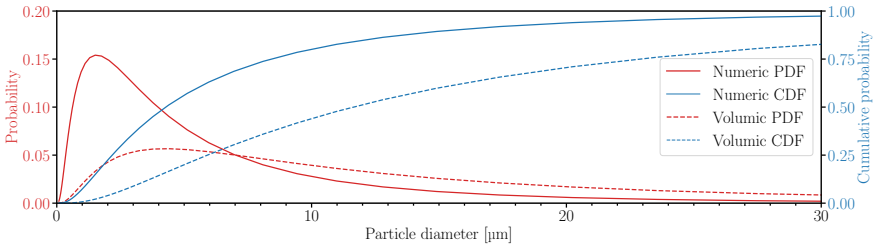

Figure 4: Numeric and volumic probability density functions (red) and cumulative density functions (blue) of the Al_2O_3 particles.

Table 4: Discretization of the distribution in 7 classes.

	Class 1	Class 2	Class 3	Class 4	Class 5	Class 6	Class 7
Represented diameters [µm]	0 - 0.5	0.5 - 1.5	1.5 - 3	3 - 6	6 - 11	11 - 19	19 - ∞
Class diameter [µm]	0.25	1	2.25	4.5	8.5	15	20
Mass flux $\left[\mathrm{kg\,s^{-1}}\right]$	0.49	4.01	6.49	8.25	5.94	3.15	2.11

defined by Boyd *et al.* [4] as in Equation (5), and the breakdown parameter B by Garcia *et al.* [34] as in Equation (6).

$$\mathrm{Kn}_{\mathrm{GLL,\,Q}} = \lambda \frac{\nabla \mathrm{Q}}{\mathrm{Q}}, \quad \mathrm{Q} \in \{T, u, \rho\} \tag{5}$$

$$\mathrm{B} = \max\left(q_i, \tau_{i,j}\right) \quad \text{with} \quad \begin{cases} q_i = \dfrac{-\kappa}{p}\sqrt{\dfrac{2m}{\mathrm{k}_B T}}\dfrac{\partial T}{\partial x_i} \\ \tau_{i,j} = \dfrac{\mu}{p}\left(\dfrac{\partial u_i}{\partial x_j} + \dfrac{\partial u_j}{\partial x_i} - \dfrac{2}{3}\dfrac{\partial u_k}{\partial x_k}\delta_{i,j}\right) \end{cases} \tag{6}$$

where μ and κ are the dynamic viscosity and thermal conductivity of the mixture, m the equivalent molecular mass, k_B the Boltzmann constant, and λ is the mean free path of the particles, computed in the continuous region as [35].

$$\lambda = \frac{\mu}{p}\sqrt{\frac{\pi \mathrm{R}_{\mathrm{specific}} T}{2}} \tag{7}$$

Since the relevancy of these parameters is still under investigation in the domain of high pressure rocket plumes at high altitude, the hypothesis of taking the maximum of all these parameters is made [13], and the rarefaction criterion Ra is therefore defined as:

$$\mathrm{Ra} = \max\left(B, \mathrm{Kn}_{\mathrm{GLL},\,u}, \mathrm{Kn}_{\mathrm{GLL},\,T}, \mathrm{Kn}_{\mathrm{GLL},\,\rho}\right) \tag{8}$$

Similar flow states have been found on the 0.05 isoline using NS and DSMC method approaches for 2D shocks and flows around cylinders [4]. However the validity of this parameter has not been proven for large scale plume flow, therefore a conservative value of $\mathrm{Ra}_{\mathrm{threshold}} = 0.01$, is used as the default and reference value for future results. The threshold value of this rarefaction parameter is also under current investigation and is further discussed in Section 3.1.2. The isoline $\mathrm{Ra} = \mathrm{Ra}_{\mathrm{threshold}}$ defines the interface between the continuous and rarefied regions. The flow solution is extracted, and in order to only have segments along which the gas velocity is outward, is smoothed using a polynomial fitting. It is then discretized into 199 segments using a total variation method on $(au_x + bu_y)/(a+b)$ quantity with $a = 1$ and $b = 3$ similar to Charton *et al.* [11].

2.4 Direct Simulation Monte-Carlo solver

The DSMC method has been developed and is extensively detailed by G.A. Bird [10]. It consists in a stochastic resolution of the Bolztmann equation which is efficient and robust for the simulation of rarefied flows. The DSMC method utilizes computational particles that serve as representations for ensembles of physical particles. It characterizes their dynamics by iteratively calculating their movements and interactions during discrete time intervals. Initially, the particle paths are determined based on their velocities, disregarding potential intersections. Then, collisions are probabilistically resolved among neighboring particles. The macroscopic properties such as velocity, density, and

temperature can be derived by conducting multiple time step samplings. In order to have an accurate and converged simulation, three main criteria shall be respected [10]:

1. Every cell size shall be less than half the local mean free path λ.
2. The simulation time step shall be less than half the smallest inter-collision time.
3. Every cell shall contain at least 10 particles of each species.

In this study the open-source code SPARTA developed by Sandia National Laboratories [36] is used. The simulations utilize the Variable Soft Sphere (VSS) collisional model [37]. A Maxwell wall condition is employed to model the interactions between particles and walls. An axial symmetry is assumed as for the NS based simulations. The simulation domain is the rectangle $(x, r) \in [-500, 300] \times [0, 800]$, in order to capture the thicker shock in front of the vehicle as well as the entire NS domain. The initial mesh consists of square elements of 40 m side, *i.e.* 20×20 squares. This initial mesh size is consistent with the mean free path in the atmosphere, which is of the order of hundreds of meters. The grid is automatically refined during the simulation based on the number of particle in each cell. A numerical Knudsen number $\mathrm{Kn}_{\mathrm{numerical}}$ is computed to ensure an appropriate spatial resolution matching the particle mean free path in high-pressure regions. This numerical Knudsen number is defined as the ratio of the local mean free path by the local cell size, with the constraint that $\mathrm{Kn}_{\mathrm{numerical}}$ shall be greater than 2 everywhere to respect criterion 1. The time step is set to 1×10^{-7} s to satisfy criterion 2 in denser regions of the flow, where the mean inter-collision time is around 2×10^{-7} s. Unless specified otherwise, the numeric representativity parameter f_{num} is 1×10^{17}, which means that every numerical particle represents 10^{17} physical particles.

Since each species in the DSMC simulation increases the computational cost due to criterion 3, only the five main species, which correspond to at least 95 % of the burnt gases molar composition, are injected at the interface for the plume (N_2, H_2, H_2O, CO, HCl) and two at the left boundary for the atmosphere (N_2, O), for a total of six species. On each injection segment, the molar fraction of each species is normalized in as follows:

$$X_{\mathrm{specie,\ normalized}} = \frac{X_{\mathrm{specie}}}{\sum_{\mathrm{species}} X_{\mathrm{species}}} \tag{9}$$

Since the DSMC domain is composed of gas at high levels of rarefaction, the hypothesis of a frozen flow is made and no chemical reactions are considered, in a similar way as Charton *et al.* [12].

3. Simulation results

3.1 Continuous flow solution validation

3.1.1 Mesh convergence

Five different meshes have been used to compute the continuous solution. The temperature field around the rocket stage is displayed in Figure 5. Figure 6a shows the temperature computed using all meshes along the $r = 0.1$ m isoline.

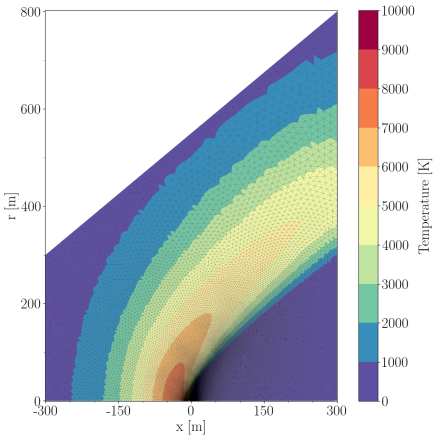

Figure 5: Temperature field around the rocket stage computed using the medium mesh.

A mean relative error is computed using the equation:

$$\mathrm{MRE}_{\mathrm{mesh}} = \sum_{n} \frac{|\mathrm{T}_{\mathrm{mesh}} - \mathrm{T}_{\mathrm{very\ fine}}|}{n\mathrm{T}_{\mathrm{very\ fine}}} \tag{10}$$

on $n = 4000$ points in a 50×5 m region downstream of the nozzle for each of the four coarser meshes. The very fine mesh used as a reference is composed of 425 000 cells. The mesh convergence is shown in Figure 6b.

Due to the high number of assumptions and models used for the simulation, as well as the computational cost of the simulation, an error smaller than 2 % is considered reasonable. The solution obtained on the *medium* mesh, which is composed of approximately 190 000 cells, is therefore usable for the interface extraction. At every point along the inside of the nozzle, the y^+ value is between 10 and 100 which matches the validity domain of the used wall law.

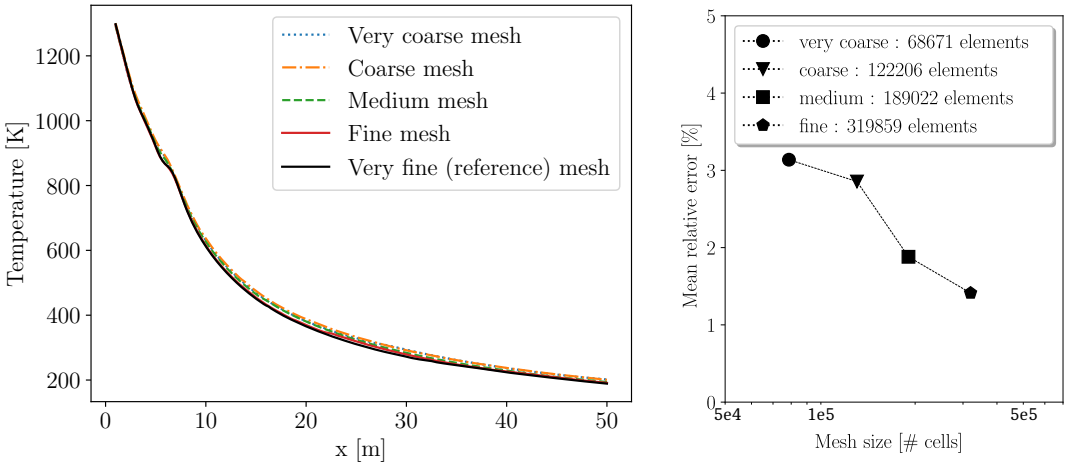

(a) (b)

Figure 6: (a) Temperature computed with all meshes along the $r = 0.1$ m isoline ; (b) mean relative error on the temperature field.

3.1.2 Validity of the particle discretization

The Weber number is defined for a liquid particle in a flow as the ratio of hydrodynamic forces from the flow on the particle and surface tension force: $\mathrm{We} = \rho\,(\Delta v)^2\,D/\sigma$, with ρ the density of the flow, Δv the relative velocity between the flow and the particle, D the diameter of the particle and σ its surface tension. The particles can fragment if $\mathrm{We} > \mathrm{We}_{\mathrm{critical}} \approx 12$ [38]. Since no fragmentation model is used for this simulation, all particles must have a We smaller than 12. The largest Δv is achieved in the throat of the nozzle since the gas accelerates more rapidly than the particles which have more inertia. At this position, the particles temperature is greater than their fusion temperature, they are therefore liquid. The Weber number of the seven particle classes along the radius of the throat are displayed in Figure 7. None of the classes reach the critical Weber number, therefore none shall fragment in the flowfield and the lack of fragmentation model can be considered as a valid hypothesis.

3.2 DSMC results sensibility in the near-lip region

The DSMC method computational cost scales linearly with the number of numerical particles in the simulation domain. The number of particles can be reduced by increasing the f_{num} parameter but a trade-off with the statistical convergence must be found and the simulation shall still comply with the criteria listed in Section 2.4. Close to the inner lip of the divergent, the mean free path of the flow is around 150 µm, which translates into having a cell size of 75 µm in this region by criterion 1. SPARTA uses a quadtree adaptive mesh refinement (AMR) method. For memory and computational cost optimization, the maximum refinement level is set to 16. If the smallest cell size is 75 µm, the biggest is around 5 m, which imposes $f_{\mathrm{num}} \leq 1.5 \times 10^{16}$ in order to satisfy criterion 3 in the farfield atmosphere. However, $f_{\mathrm{num}} \leq 1.5 \times 10^{17}$ is sufficient to satisfy criterion 3 close to the lip due to the density of the flow.
A method to reduce the computational cost of a full scale simulation is therefore to increase the minimum cell size in the simulation domain. Several methods to achieve this goal are assessed in the following.

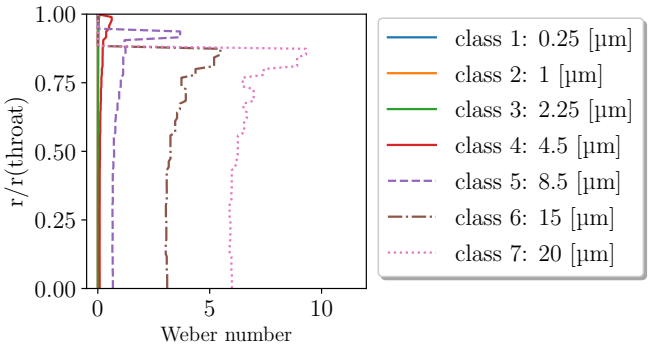

Figure 7: Weber number along the radius of the throat for each particle class defined in Table 4.

In order to reduce the computational cost of these test cases, a smaller domain $\mathrm{d}x \times \mathrm{d}y = 1.5 \times 3\,\mathrm{m}$ depicted in Figure 8 (c) is simulated. The state of the interface is extracted from the continuous based simulation described in Section 3.1. In order to simplify these test cases, the atmospheric flow is not taken into account. All other parameters are similar to those in Section 2.4.

For each test case, the error is defined for all view angles ν along the thick dashed lines of Figure 8 (c). The error is computed on the boundary of the domain to reduce the effects of different discretization of the interface using the total variation method, which could have some effect close to the interface. The error is not computed for high view angles (*i.e.* on the lower x boundary) because not enough particles are present in this zone to satisfy the criterion 3 and the errors would be meaningless. The error metric is defined as the relative error on the Mach field between two configurations A and B as:

$$\text{Relative error} = \frac{\mathrm{Ma}_{\text{configuration A}} - \mathrm{Ma}_{\text{configuration B}}}{\mathrm{Ma}_{\text{configuration B}}} \tag{11}$$

Figure 9 to Figure 11 represent the error for all configurations.

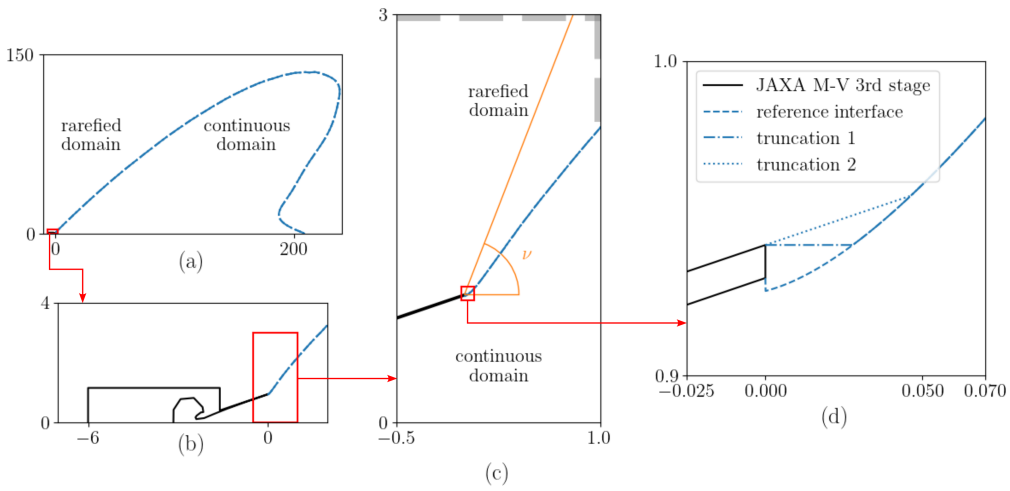

Figure 8: (a) Rocket stage (black) and Ra= 0.01 isoline (blue) ; (b) close-up view of the stage ; (c) simulation domain for the near-lip simulations ; (d) close-up view of the near-lip region. The red arrows going from one subfigure to the next indicate a zoom. Dimensions are in meters.

Considering the smallest mean free path λ is located close to the inner side of the divergent lip, a first possibility to increase the minimum cell size is to make a geometric truncation of the interface as depicted in Figure 8 (d). This region is critical because it is composed of numerous particles with a small mean free path and is therefore extremely costly to simulate using the DSMC method. The truncation 1 consists in an horizontal cut of the interface so that only $y > y_{\text{lip}}$ is simulated using the DSMC method. The truncation 2 is similar but with a slended cut with the same slope as the outer divergent. The relative error between the reference interface and both truncation is depicted in Figure 9. Downstream of the rocket stage, the relative error on the Mach field induced by these truncation is less than 5 %, but the error increases upstream which makes these truncation not suitable for heat and particle fluxes simulation on the

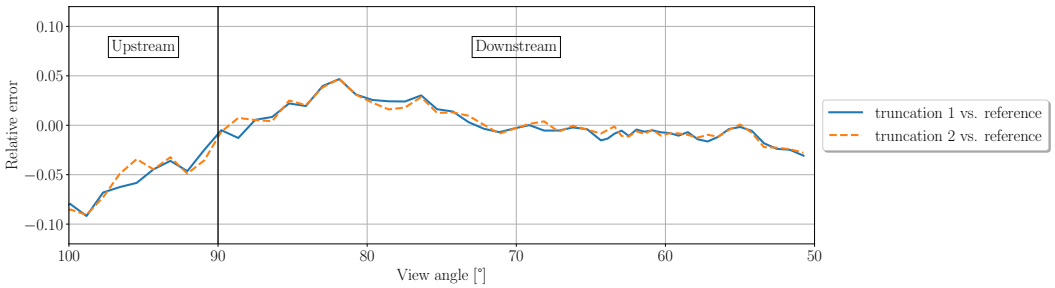

Figure 9: Relative error on the Mach field as a function of the view angle for between the two truncations and the reference interface.

outside wall of the rocket. Similar results are obtained if the error is computed using the density or temperature instead of the Mach number. Truncations 1 and 2 return extremely close flowfields. Even though truncation 1 reduces the computation time compared to the reference interface, it is still computationally heavier than truncation 2 and does not induce smaller errors. Therefore if the computational cost is a critical matter truncation 2 shall be used, and if minimization of the error is preferred the reference interface shall be used.

Another way to increase the minimum cell size is to limit the AMR in SPARTA, therefore breaking criterion 1. Four configurations have been assessed:

1. The smallest cell size is increased from 75 µm to 300 µm for the reference interface.
2. The smallest cell size is increased from 75 µm to 600 µm for the reference interface.
3. The smallest cell size is increased from 150 µm to 300 µm for truncation 2.
4. The smallest cell size is increased from 150 µm to 600 µm for truncation 2.

In each case the only region where the smallest cells are present is close to the lip of the divergent. The error on the Mach field along a range of view angles is depicted in Figure 10, and is less 3 % everywhere for both bigger cell sizes. Since the error alternates between positive and negative values in a seemingly random manner, it is suspected

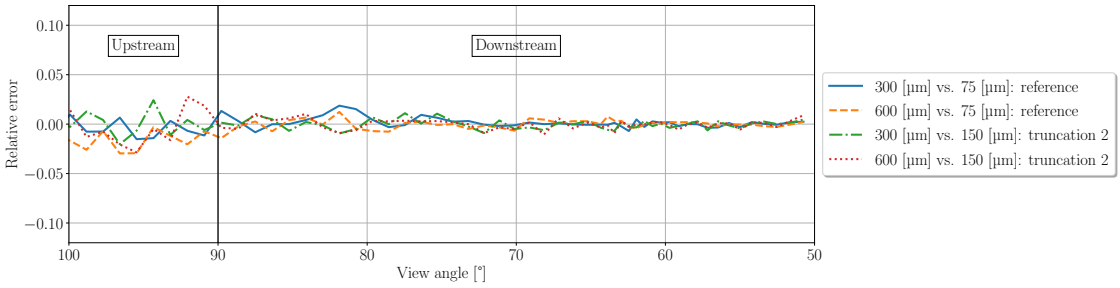

Figure 10: Relative error on the Mach field as a function of the view angle for increased minimum cell sizes.

that this error is due to lack of statistical convergence. The hypothesis to explain such a low error is that the region where criterion 1 is not respected is small and the particles have a large velocity, therefore they do not stay long in the non converged region and the effect on the resulting flowfield is negligible. Considering the error is smaller using 600 µm cells with the reference interface, *i.e.* the dashed line in Figure 10, than using 150 µm cells with the truncated interface, *i.e.* the dashed line in Figure 9, it seems preferable to perform the full scale simulation using no truncation and a minimum cell size increased to 600 µm.

Finally, the minimum cell size can be increased by raising the threshold value of the rarefaction criterion $\mathrm{Ra}_{\mathrm{threshold}}$. Figure 11 shows the relative error on the Mach number between $\mathrm{Ra}_{\mathrm{threshold}} = 0.03$, $\mathrm{Ra}_{\mathrm{threshold}} = 0.01$ and $\mathrm{Ra}_{\mathrm{threshold}} = 0.005$ which is taken as the reference. Surprisingly, the error exceeds 5 % even for the $\mathrm{Ra}_{\mathrm{threshold}} = 0.01$ simulation. The $\mathrm{Ra}_{\mathrm{threshold}} = 0.03$ case exceeds a 10 % error at high view angles. Two hypotheses can be made to explain this results. First, it is possible that a threshold value of 0.01 is too large in that case to be in the validity domain of the NS equations. Secondly, these errors could also be due to a lack of convergence in the NS simulation mesh. Indeed, even if the NS simulation is converged on a global scale, the high view angles are driven almost exclusively by the flow near the lip of the divergent which may not be captured well enough with the current mesh.

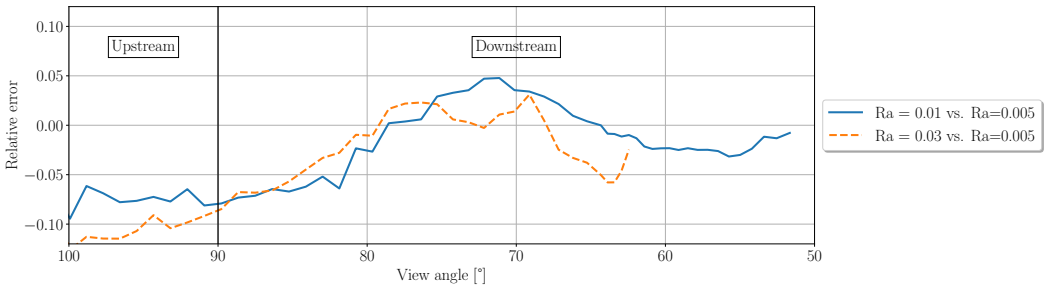

Figure 11: Relative error on the Mach field as a function of the view angle between for different threshold values of the rarefaction criterion.

3.3 Full-scale one-way NS-DSMC simulation

Based on the sensitivity study, the full scale simulation using the DSMC method is done using as interface a discretization into 199 segments of the Ra = 0.01 reference interface, with a limitation in the minimum cell size to 600 µm. The total number of particles simulated in the domain once convergence is reached is around 775×10^6, and the mesh is composed of 7.2×10^6 cells. The simulation has been performed using 840 CPU cores during 195 hours, *i.e.* around 164 000 CPU-hours. The statistical means are computed using 50 000 time steps, which corresponds to a total averaging time of 5×10^{-3} s. Figure 12 presents the comparison between the NS simulation at the bottom of every subplot and the hybrid NS-DSMC simulation at the top. Even if the mesh appears coarse in the atmosphere, it respects the three criteria given in Section 2.4.

First, the standalone NS simulation fails to capture the correct expansion of light species in the upstream direction as the DSMC method does. In Figure 12a, the lightest species H_2 is blown towards the front of the vehicle in the DSMC simulation. Its molecular fraction even reaches values larger than 0.9, whereas in the NS simulation the molar fraction is more homogeneous and decreases smoothly up to the atmospheric value compared to the DSMC. A DSMC simulation seems to be mandatory if the flow properties at the external wall are of interest.

Secondly, the NS and hybrid NS-DSMC solutions do not predict the same temperature inside the shock, as shown in Figure 12b. In the former the peak temperature is reached along the symmetry axis a few meters in front of the vehicle, whereas in the latter it is reached at an offset of around 100 m from the axis. This behaviour was highly unexpected and shall be investigated further in future works. The NS solution is expected to be wrong upstream of the vehicle due to the rarefied aspect of the atmosphere, but the lack of convergence in the DSMC method does not allow for firm conclusions on the physical temperature to be made. If this phenomenon were to be physical, an hypothesis to explain it would be the difference of chemical composition, due to H_2 expansion for instance, between the front of the vehicle, *i.e.* view angles of more than 80°, and smaller view angles. The total temperature of H_2 is lower than that of the atmosphere, which could explain why the peak temperature is not located on the axis. This hypothesis shall need further investigation.

The density and Mach number displayed in respectively Figure 12c and Figure 12d are in good agreement between the NS and the hybrid NS-DSMC simulation inside the plume at low view angles. Figure 13a shows the Mach number as a function of the view angle, and it is clear that in the core of the plume the standalone NS solution is similar to the hybrid NS-DSMC one. Figure 13b represents, in the same way as Figure 9 to Figure 11, the relative difference between the NS solution and the hybrid solution, which is taken as a reference value. Up to 35°, the flows from the NS and hybrid methods at 300 m from the divergent are at most 10 % apart. Outside of the range, and particularly in the 35° to 60° range which corresponds to the shock, the difference between the two methods is large. This result is expected since the shock is a region of high thermodynamic non-equilibrium that the NS equations cannot properly capture. Everywhere $\mathrm{Ra} < \mathrm{Ra}_{\mathrm{threshold}} = 0.015$, which corresponds to the isoline with an angle of 35°, can be simulated using the NS equations while retaining an error of less than 10 %. This value is smaller than those in the literature, which are around 0.05 [4]. Future work investigating why this threshold value seems not to be universal shall be done.

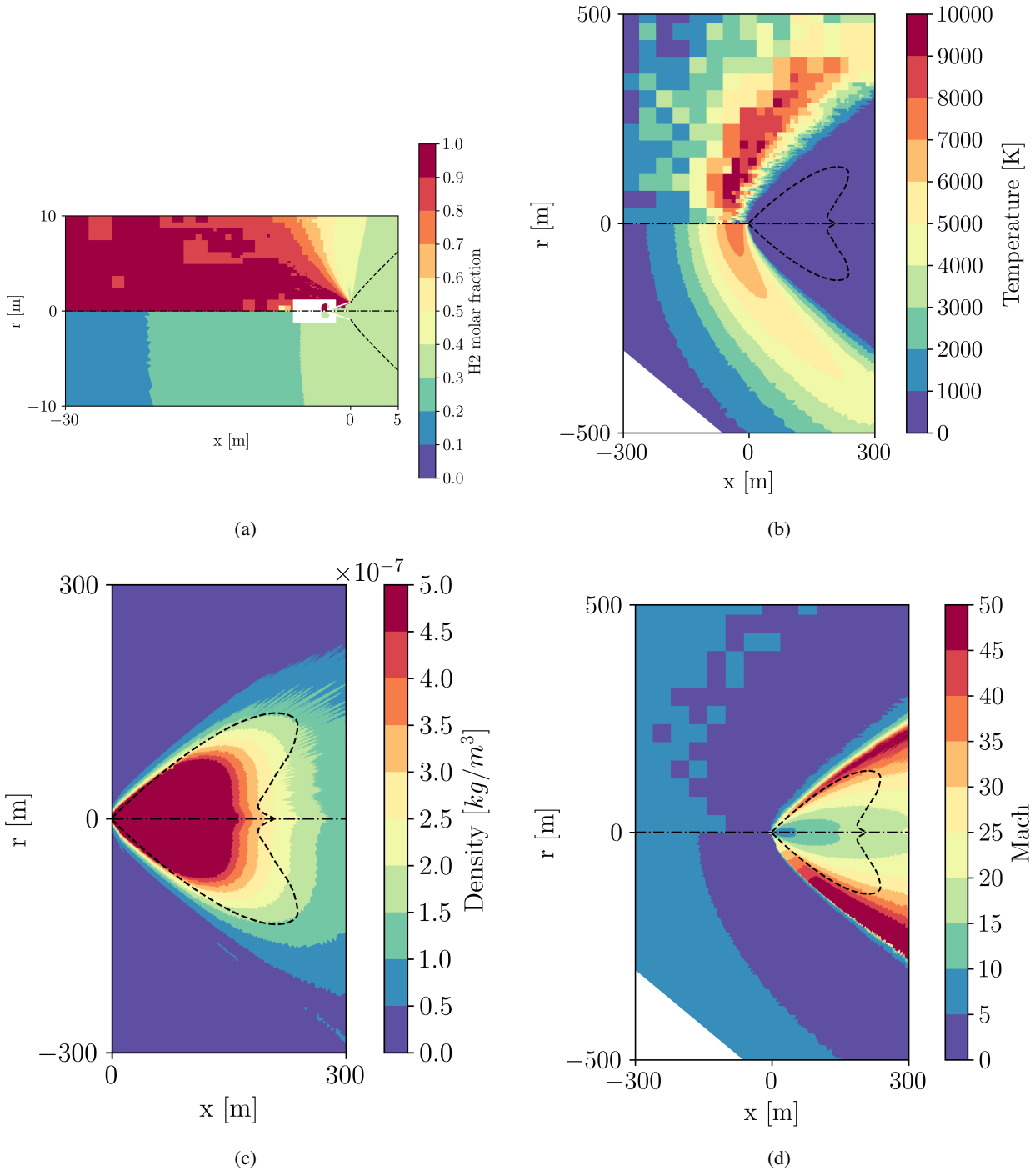

Figure 12: One-way NS-DSMC simulation results (top) vs. NS only simulation results (bottom) for (a) H_2 molar fraction ; (b) temperature ; (c) density ; (d) Mach number. The interface is plotted in dashed line and the symmetry axis in dotted dash. The zone delimited by the interface, *i.e.* corresponding to the continuous domain in Figure 8, is simulated only using NS.

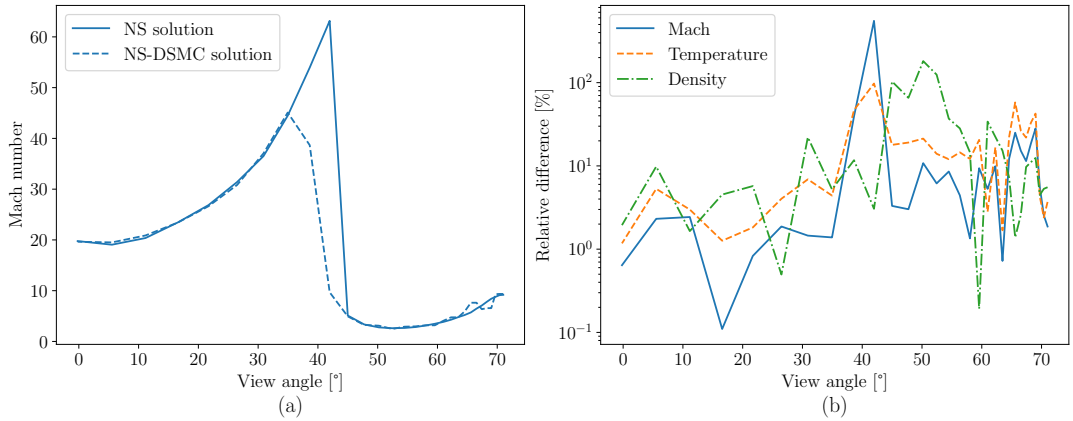

Figure 13: (a) Mach field on as a function of the view angle from the right boundary of the domain, for both the standalone NS solution and the Hybrid NS-DSMC solution ; (b) relative difference on several state variables as a function of the view angle on the right boundary of the domain.

4. Conclusion

In this paper, a one-way hybrid NS-DSMC methodology has been applied to a full-scale simulation of the JAXA's M-V third stage. A simulation with a CFD solver based on the Navier-Stokes equations was first performed. An interface delimiting the validity domain of these equations and defined as an isoline of a rarefaction parameter Ra was then extracted. This interface was used as an input condition for a Boltzmann based simulation relying on the Direct-Simulation Monte-Carlo method. From these results a more precise range of validity of the NS equations in the context of rocket plumes at high altitude has been determined.

The lack of capture by the NS equations of several state phenomena, particularly ahead of the stage, has also been presented. This includes the expansion of volatile species such as H_2, the temperature in the shock and the shock thickness for instance. Several issues arose due to the multiphysics and multiscale aspect of the case, which were not present in previous works [11, 12]. The numerical limitations due to having several orders of magnitude of difference in densities between the farfield atmosphere and the near-lip region were tackled by limiting the minimum cell size in the denser regions and this hypothesis was validated on simple cases. Chemical reactions in the rarefied domain were not taken into account but shall be in future works to compute the electron density downstream of the stage.

The influence of several parameters on the simulation results, such as the NS mesh cell size in the near-lip region, the parameters used in the computation of Ra, or the Ra threshold value shall be further investigated.

5. Acknowledgments

The authors would like to thank the French Defense Innovation Agency (AID), the French Procurement Agency for Armament (DGA) and the ONERA's scientific direction for funding and supporting the present work.

References

[1] K. Kinefuchi, K. Okita, I. Funaki, and T. Abe. "Prediction of in-flight radio frequency attenuation by a rocket plume". In : *Journal of Spacecraft and Rockets* 52.2 (Mar. 2015), pp. 340–349. DOI: 10.2514/1.a32957.

[2] S. Smith. "Improvements in rocket engine nozzle and high altitude plume computations". In : (July 1983). DOI: 10.2514/6.1983-1547.

[3] A. Langenais, F. Vuillot, J. Troyes, and C. Bailly. "Accurate simulation of the noise generated by a hot supersonic jet including turbulence tripping and nonlinear acoustic propagation". In : *Physics of Fluids* 31.1 (Jan. 2019), p. 016105. DOI: 10.1063/1.5050905.

[4] I. D. Boyd, G. Chen, and G. V. Candler. "Predicting failure of the continuum fluid equations in transitional hypersonic flows". In : *Physics of Fluids* 7.1 (Jan. 1995), pp. 210–219. DOI: 10.1063/1.868720.

[5] A. Agrawal, H. M. Kushwaha, and R. S. Jadhav. *Burnett Equations: Derivation and Analysis*. Springer International Publishing, May 2019, pp. 125–188. DOI: 10.1007/978-3-030-10662-1_5.

[6] G. V. Candler, S. Nijhawan, D. Bose, and I. D. Boyd. "A multiple translational temperature gas dynamics model". In : *Physics of Fluids* 6.11 (Nov. 1994), pp. 3776–3786. DOI: 10.1063/1.868367.

[7] P. L. Bhatnagar, E. P. Gross, and M. Krook. "A Model for Collision Processes in Gases. I. Small Amplitude Processes in Charged and Neutral One-Component Systems". In : *Physical Review* 94.3 (May 1954), pp. 511–525. DOI: 10.1103/PhysRev.94.511.

[8] C. R. Justiz, R. M. Sega, C. Dalton, and A. Ignatiev. "DSMC- and BGK-based calculations for return flux contamination of an outgassing spacecraft". In : *Journal of Thermophysics and Heat Transfer* 8.4 (Oct. 1994), pp. 802–803. DOI: 10.2514/3.617Âă.

[9] C. Baranger, Y. Dauvois, G. Marois, J. Mathé, J. Mathiaud, and L. Mieussens. "A BGK model for high temperature rarefied gas flows". In : *European Journal of Mechanics - B/Fluids* 80 (Mar. 2020), pp. 1–12. DOI: 10.1016/j.euromechflu.2019.11.006.

[10] G. A. Bird. *Molecular Gas Dynamics and the Direct Simulation of Flows*. Oxford Univerity Press, 1994.

[11] V. Charton, A. Awad, and J. Labaune. "Optimisation of a hybrid NS–DSMC methodology for continuous–rarefied jet flows". In : *Acta Astronautica* 195 (June 2022), pp. 295–308. DOI: 10.1016/j.actaastro.2022.03.012.

[12] V. Charton, A. Langenais, and J. Labaune. "High altitude rocket reactive jet flow simulations with a hybrid NS-DSMC methodology". In : *EUCASS2022*. Proceedings of the 9th European Conference for Aerospace Sciences. Lille, France, 27 June - 1 July, 2022. DOI: 10.13009/EUCASS2022-7245.

[13] U. Rasthofer, P. Ohmer, and H. Siegmann. "A Hybrid Continuum-Kinetic Approach for High Altitude Rocket Exhaust Plume Simulation". In : *Use of Computational Fluid Dynamics for Design and Analysis: Bridging the Gap Between Industry and Developers*. STO, June 2022.

[14] T. E. Schwartzentruber and I. D. Boyd. "A hybrid particle-continuum method applied to shock waves". In : *Journal of Computational Physics* 215.2 (July 2006), pp. 402–416. DOI: 10.1016/j.jcp.2005.10.023.

[15] I. Nompelis, M. D. Kroells, T. E. Schwartzentruber, and G. V. Candler. "Towards a Fully Consistent DSMC-CFD Hybrid Method for Hypersonic Nonequilibrium Reacting Flows". In : *AIAA SCITECH 2023 Forum*. American Institute of Aeronautics and Astronautics, Jan. 2023. DOI: 10.2514/6.2023-2136.

[16] G. Abbate, B. J. Thijsse, and C. R. Kleijn. "Validation of a Hybrid Navier-Stokes/DSMC Method for Multiscale Transient and Steady-State Gas Flows". In : *International Journal for Multiscale Computational Engineering* 6.1 (2008), pp. 1–12. DOI: 10.1615/IntJMultCompEng.v6.i1.10.

[17] Z. Tang, B. He, and G. Cai. "Investigation on a coupled Navier-Stokes-Direct Simulation Monte Carlo method for the simulation of plume flowfield of a conical nozzle". In : *International Journal for Numerical Methods in Fluids* 76.2 (July 2014), pp. 95–108. DOI: 10.1002/fld.3924.

[18] Z. Yang, Z.-Y. Tang, G.-B. Cai, and B.-J. He. "Development of a coupled NS-DSMC method for the simulation of plume impingement effects of space thrusters". In : *Thermophysics and Aeromechanics* 24.6 (Nov. 2017), pp. 835–847. DOI: 10.1134/s0869864317060026.

[19] J. Papp, R. Wilmoth, C. Chartrand, and S. Dash. "Simulation of High-Altitude Plume Flow Fields Using a Hybrid Continuum CFD/DSMC Approach". In : *42nd AIAA/ASME/SAE/ASEE Joint Propulsion Conference & Exhibit*. American Institute of Aeronautics and Astronautics, July 2006. DOI: 10.2514/6.2006-4412.

[20] G. Cai, L. Liu, B. He, G. Ling, H. Weng, and W. Wang. "A Review of Research on the Vacuum Plume". In : *Aerospace* 9.11 (Nov. 2022), p. 706. DOI: 10.3390/aerospace9110706.

[21] V. Ghazanfari, M. M. Shademan, and F. Mansourzadeh. "Investigation of feed flow effect using CFD-DSMC method in a gas centrifuge". In : *Journal of Nuclear Research and Applications* 2.4 (Oct. 2022), pp. 7–14. DOI: 10.24200/jon.2022.1027.

[22] K. Kinefuchi, H. Yamaguchi, M. Minami, K. Okita, and T. Abe. "In-flight S-band telemetry attenuation by ionized solid rocket motor plumes at high altitude". In : *Acta Astronautica* 165 (Dec. 2019), pp. 373–381. DOI: 10.1016/j.actaastro.2019.09.025.

[23] JAXA. *Japan Aerospace Exploration Agency Special Document (ISSN 1349-113X – JAXA-SP-07-023)*. Tech. rep. Japan Aerospace Exploration Agency, Feb. 2008.

[24] A. Refloch, B. Courbet, A. Murrone, P. Villedieu, C. Laurent, P. Gilbank, J. Troyes, L. Tessé, G. Chaineray, J. B. Dargaud, et al. "CEDRE Software". In : *Aerospace Lab* 2 (2011), pp. 1–10.

[25] D. Scherrer, F. Chedevergne, P. Grenard, J. Troyes, A. Murrone, E. Montreuil, F. Vuillot, N. Lupoglazoff, M. Huet, B. Sainte-Rose, et al. "Recent CEDRE Applications". In : *Aerospace Lab* 2 (2011), pp. 1–28.

[26] M. Smoluchowski. "Ueber Wärmeleitung in verdünnten Gasen". In : *Annalen der Physik* 300.1 (1898), pp. 101–130. DOI: 10.1002/andp.18983000110.

[27] H. Struchtrup. *Macroscopic transport equations for rarefied gas flows: approximation methods in kinetic theory (interaction of mechanics and mathematics)*. Interaction of Mechanics and Mathematics. Springer, 2005. ISBN: 3540245421.

[28] F. La Torre, S. Kenjereš, J.-L. Moerel, and C. R. Kleijn. "Hybrid simulations of rarefied supersonic gas flows in micro-nozzles". In : *Computers Fluids* 49.1 (Oct. 2011), pp. 312–322. DOI: 10.1016/j.compfluid.2011.06.008.

[29] USAF. *U.S. Standard Atmosphere*. Tech. rep. NOAA, NASA, USAF, 1976.

[30] M. Capitelli, C. M. Ferreira, B. F. Gordiets, and A. I. Osipov. *Plasma Kinetics in Atmospheric Gases*. Ed. by Springer Science Business Media. 2013. ISBN: 3662041588, 9783662041581.

[31] Q. Binauld. "Modélisation et simulation du rayonnement dans les jets de moteurs à propergol solide à haute altitude". PhD thesis. Université Paris-Saclay, 2018.

[32] V. Rialland, A. Guy, D. Gueyffier, P. Perez, A. Roblin, and T. Smithson. "Infrared signature modelling of a rocket jet plume - comparison with flight measurements". In : *Journal of Physics: Conference Series* 676 (Jan. 2016), p. 012020. DOI: 10.1088/1742-6596/676/1/012020.

[33] R. W. Hermsen. "Aluminum Oxide Particle Size for Solid Rocket Motor Performance Prediction". In : *Journal of Spacecraft and Rockets* 18.6 (Nov. 1981), pp. 483–490. DOI: 10.2514/3.57845.

[34] A. L. Garcia and B. J. Alder. "Generation of the Chapman-Enskog distribution". In : *Journal of computational physics* 140.1 (May 1998), pp. 66–70.

[35] W. G. Vincenti and C. H. Kruger. *Introduction to Physical Gas Dynamics*. 2nd. Krieger Publlishing Company, 1975. ISBN: 978-0882753096.

[36] S. J. Plimpton, S. G. Moore, A. Borner, A. K. Stagg, T. P. Koehler, J. R. Torczynski, and M. A. Gallis. "Direct Simulation Monte Carlo on petaflop supercomputers and beyond". In : *Physics of Fluids* 31.8 (Aug. 2019), p. 086101. DOI: 10.1063/1.5108534.

[37] I. D. Boyd and T. E. Schwartzentruber. *Nonequilibrium Gas Dynamics and Molecular Simulation*. Cambridge University Press, Mar. 2017. 384 pp. ISBN: 978-1-107-07344-9.

[38] M. Pilch and C. A. Erdman. "Use of breakup time data and velocity history data to predict the maximum size of stable fragments for acceleration-induced breakup of a liquid drop". In : *International Journal of Multiphase Flow* 13.6 (Nov. 1987), pp. 741–757. DOI: 10.1016/0301-9322(87)90063-2.